

## CAPILLARY END EFFECTS IN COREFLOOD CALCULATIONS

David D. Huang and Matt M. Honarpour

Mobil Technology Company, 13777 Midway Road, Dallas, 75244, USA

This paper was prepared for presentation at the 1996 International Symposium of the Society of Core Analysts held in Montpellier, France, September 8-10, 1996.

### ABSTRACT

Capillary end effects in coreflood experiments, in some cases, can significantly influence the computation of end-point relative permeabilities and final saturation levels. Because capillary end effects arise from capillarity, these corrections for relative permeability and saturation can be quantified if the capillary pressure curve is known *a priori*. Based on Darcy's law and the relative permeability-capillary pressure relationships, we present in this paper how these corrections can be done in corefloods if the *in-situ* saturation profile is unavailable. Under the same principle, if the *in-situ* saturation profile of the capillary end is available, it is therefore possible to simultaneously predict both relative permeability and capillary pressure using pressure data. Such a method of prediction is presented in the paper and experimentally verified. In a reservoir-conditioned oilflood using a carbonate core sample, we obtained the capillary end information through *in-situ* microwave monitoring, and the relative permeability and capillary pressure were predicted based on the theory. The predictions were compared with separate capillary pressure (mercury injection, porous-plate, and centrifuge) and relative permeability (steady-state) measurements. The predictions and experiments agree well with one another.

### INTRODUCTION

The capillary end effect is an important issue in coreflood experiments, because it can cause serious errors in the calculation of saturation and relative permeabilities from pressure drop and production information. Capillary end effects arise from the discontinuity of capillarity in the wetting phase at the outlet end of the core sample.

Capillary end effects commonly appear in situations of oil displacing water in water-wet cores, and gas-displacing-oil cases. In other displacement processes, capillary end effects are less pronounced than these two situations. Experiments of oil displacing water in a water-wet core, or a *drainage process*, are important, because they establish the end-point oil relative permeability at the interstitial water saturation,  $k_{ro} @ S_{iw}$ , which is the starting point of a waterflood (or an *imbibition*) process. Experiments of the gas-displacing-oil cases are also important, because they represent internal or external gas displacement in oil reservoirs.

This paper shows how to correct errors in saturation and relative permeabilities exploiting the capillary end effect. With this theory, we will show how to estimate relative permeability and capillary pressure simultaneously from *in-situ* capillarity information.

**The Capillary End Effect Formulation** - For the purpose of illustration, we discuss an experiment of co-injecting oil and water into a water-presaturated, water-wet core sample. The saturation profiles during the experiments are schematically shown in Fig.1. After oil breakthrough, the system approaches steady-state ( $t \rightarrow \infty$ ), and water capillarity tends to keep a higher water saturation toward the core end. This non-uniform saturation profile at the steady-state is called the *capillary end effect*, and can be formulated based on Darcy's law for both the fluids:

$$\frac{q_w}{A} = - \frac{k k_{rw}}{\mu_w} \frac{\partial p_w}{\partial x} \quad (1)$$

$$\frac{q_o}{A} = - \frac{k k_{ro}}{\mu_o} \frac{\partial p_o}{\partial x} \quad (2)$$

where  $A$  is the core cross-sectional area ( $\text{cm}^2$ ),  $k$  the absolute permeability (md),  $k_{rw}$  and  $k_{ro}$  the relative permeabilities (dimensionless),  $q_w$  and  $q_o$

the flow rates (cm<sup>3</sup>/sec),  $\mu_w$  and  $\mu_o$  the fluid viscosities (g/cm-sec or Poise),  $p_w$  and  $p_o$  the phase pressures (g/cm-sec<sup>2</sup> or dyne/cm<sup>2</sup>), and  $x$  the distance from the inlet end (cm).

Water-oil capillary pressure is

$$P_c = p_o - p_w \quad (3)$$

Combining Eqs.(1)-(3) gives

$$\frac{1}{kA} \left( \frac{q_w \mu_w}{k_{rw}} - \frac{q_o \mu_o}{k_{ro}} \right) = \frac{\partial P_c}{\partial x} \quad (4)$$

Since the capillary pressure is only a function of water saturation, the right-hand term of Eq.(4) can be written as

$$\frac{\partial P_c}{\partial x} = \frac{dP_c}{dS_w} \frac{\partial S_w}{\partial x} \quad (5)$$

Eqs.(4) and (5) together give

$$\frac{\partial S_w}{\partial x} = \frac{1}{kA} \left( \frac{q_w \mu_w}{k_{rw}} - \frac{q_o \mu_o}{k_{ro}} \right) \Big/ \frac{dP_c}{dS_w} \quad (6)$$

At steady-state ( $t \rightarrow \infty$ ), water saturation is not a function of time, thus

$$\frac{dS_w}{dx} = \frac{1}{kA} \left( \frac{q_w \mu_w}{k_{rw}} - \frac{q_o \mu_o}{k_{ro}} \right) \Big/ \frac{dP_c}{dS_w} \quad (7)$$

(steady state)

This equation can be integrated if all quantities are known (that is  $k_{ro}$ ,  $k_{rw}$ , and  $P_c$  are known functions of  $S_w$ ;  $q_w$ ,  $q_o$ ,  $\mu_w$ ,  $\mu_o$ ,  $k$ ,  $A$  are all known). The integration results predict the steady-state saturation profile as a function of distance,

$$L - x = \int_x^L dx = kA \int_{S_w}^{S_{w,out}} \left[ \frac{dP_c}{dS_w} \Big/ \left( \frac{q_w \mu_w}{k_{rw}} - \frac{q_o \mu_o}{k_{ro}} \right) \right] dS_w \quad (8)$$

In this equation,  $L - x$  represents the distance from the core outlet. The upper limit in the integration on the right-hand side is the water saturation at the core outlet end. In a water-wet system, a relatively large amount of water may be withheld toward the core outlet because of the capillarity. Therefore, without causing much error,  $S_{w,out}$  can either be assumed as 100% in the absence of residual oil, or  $1 - S_{or}$  in the presence of residual oil. Eq.(8) can be subsequently written as

$$L - x = \int_x^L dx = kA \int_{S_w}^{1-S_{or}} \left[ \frac{dP_c}{dS_w} \Big/ \left( \frac{q_w \mu_w}{k_{rw}} - \frac{q_o \mu_o}{k_{ro}} \right) \right] dS_w$$

(steady-state, water-wet, oil/water system) (9)

If initially there is no residual oil,  $S_{or}$  is set to zero in the above equation. Since Eq.(9) governs the saturation profile, we will refer it to as the "profile equation."

### Previous Theoretical/Experimental Work

Richardson *et al*<sup>1</sup> conducted a series of gas-displacing-oil experiments using a Berea sandstone to study capillary end effects. The oil saturation in all experiments was initially 100%. Thus, for gas/oil system, the profile equation is

$$L - x = kA \int_{S_o}^1 \left[ \frac{dP_c}{dS_o} \Big/ \left( \frac{q_o \mu_o}{k_{ro}} - \frac{q_g \mu_g}{k_{rg}} \right) \right] dS_o$$

(steady-state, gas/oil system, initially  $S_o = 100\%$ ) (10)

Richardson *et al*<sup>1</sup> compared their experimental results with that predicted by Eq.(10), and demonstrated excellent agreements between measurements and predictions. Their results support the theoretical profile equation.

### THE CAPILLARY END EFFECT BY THE COREY-BURDINE EQUATION

We return to the oil-displacing-water situation. Brooks and Corey<sup>2</sup> assumed that the capillary pressure can be represented by

$$P_c = P_d \left( \frac{S_w - S_{iw}}{1 - S_{iw} - S_{or}} \right)^{-\frac{1}{\lambda}} \quad (11)$$

where  $P_d$  is the displacement pressure (sometimes called "threshold pressure"), and  $\lambda$  is a material constant determined experimentally. Eq.(11) is schematically shown in Fig.2.

In Fig.2, the mobile saturation range is  $1 - S_{iw} - S_{or}$ ; we define normalized water saturation as

$$S_w^* = \frac{S_w - S_{iw}}{1 - S_{iw} - S_{or}} \quad (12)$$

and Eq.(11) becomes

$$P_c = P_d (S_w^*)^{-\frac{1}{\lambda}} \quad (13)$$

Based on the work of Purcell<sup>3</sup>, Corey combined Burdine's research<sup>4</sup> on tortuosity and developed the *Corey-Burdine Equations*<sup>5-6</sup>. For oil-water systems, the Corey-Burdine equations predict the following interrelationships between relative permeabilities and capillary pressure:

$$k_{ro} = k_{ro}|_{S_{iw}} (1 - S_w^*)^2 \left[ \frac{\int_{S_w^*}^1 \frac{dS_w^*}{P_c^2}}{\int_0^1 \frac{dS_w^*}{P_c^2}} \right] \quad (14)$$

$$k_{rw} = k_{rw}|_{S_{or}} (S_w^*)^2 \left[ \frac{\int_0^{S_w^*} \frac{dS_w^*}{P_c^2}}{\int_0^1 \frac{dS_w^*}{P_c^2}} \right] \quad (15)$$

Substituting Eq.(13) into Eqs.(14) and (15), Brooks and Corey<sup>2</sup> obtained the following results:

$$k_{ro} = k_{ro}|_{S_{iw}} (1 - S_w^*)^2 [1 - (S_w^*)^{\lambda+1}] \quad (16)$$

$$k_{rw} = k_{rw}|_{S_{or}} (S_w^*)^{\lambda+3} \quad (17)$$

With these expressions, the profile equation, Eq.(9), becomes

$$\frac{L-x}{L} = \frac{k k_{ro}|_{S_{iw}} AP_d}{Lq_o \mu_o} \left\{ \frac{1}{\lambda} \int_{S_w^*}^1 \frac{(S_w^*)^{\frac{1}{\lambda}+2} (1-S_w^*)^2 [1 - (S_w^*)^{\lambda+1}]}{(S_w^*)^{\lambda+3} - \frac{k_{ro}|_{S_{iw}} q_w \mu_w}{k_{rw}|_{S_{or}} q_o \mu_o} (1-S_w^*)^2 [1 - (S_w^*)^{\lambda+1}]} dS_w^* \right\} \quad (18)$$

which applies to steady-state oil-displacing-water situations in a water-wet core.

Ideally, one would integrate Eq.(18) to obtain the steady-state saturation profile,  $S_w$  as a function of distance, in an oil-displacing-water experiment. Realistically, this equation is difficult to use. In this equation,  $P_d$  and  $\lambda$  can be determined by a capillary pressure experiment; the terminal water relative permeability,  $k_{rw}|_{S_{iw}}$ , can be determined by a water-displacing-oil (*i.e.*, a waterflood) experiment, assuming no capillary end effects if the core is rendered water-wet. The only term causing problem is the terminal oil relative permeability,  $k_{ro}|_{S_{iw}}$ , which cannot be evaluated *a priori* in an experiment. The reason is that one gets the value of an *averaged* oil relative permeability ( $\bar{k}_{ro}$ ) at an *averaged* terminal

condition ( $\bar{S}_{iw}$ ) based on the pressure drop over the whole core and the water production. In other words,  $k_{ro}|_{S_{iw}}$  is a part of the solution, not a known parameter.

Our goals are to compute the *actual* terminal oil relative permeability ( $k_{ro}|_{S_{iw}}$ ) and the *actual* water saturation ( $S_{iw}$ ) values from the averaged  $\bar{k}_{ro}|_{\bar{S}_{iw}}$  and  $\bar{S}_{iw}$ . In the next section, we will show step by step how this can be accomplished.

Using the word "actual" does not mean "true" values of relative permeability and saturations, which should be directly measured in the absence of capillary end effects. "Actual," in our phrase, means derived values, where the use of the Corey-Burdine Equations and the idealized capillary pressure curve (Eq.(11)) are implicit.

### ERROR CORRECTION IN RELATIVE PERMEABILITY AND SATURATION CALCULATIONS

We consider the oil-displacing-water case again. The calculations presented in this work can be as well extended to other coreflood situations such as the gas-displacing-oil cases, provided that the subscripts are appropriately changed ( $w$  to  $o$  and  $o$  to  $g$ ). For example, change the  $k k_{ro}|_{S_{iw}} AP_d / Lq_o \mu_o$  term in our work to  $k k_{rg}|_{S_{iw}} AP_d / Lq_g \mu_g$  for a gas-displacing-oil case, where  $P_d$  becomes the displacement pressure (a positive value) for gas displacing oil.

To further simplify our discussion, we consider the scenarios of single-phase oil injection. Setting  $q_w = 0$  (no water co-injection) in Eq.(18):

$$\frac{L-x}{L} = \frac{k k_{ro}|_{S_{iw}} AP_d}{Lq_o \mu_o} \frac{1}{\lambda} \times \int_{S_w^*}^1 \left\{ (1-S_w^*)^2 [1 - (S_w^*)^{\lambda+1}] / (S_w^*)^{\frac{1}{\lambda}+1} \right\} dS_w^* \quad (19)$$

(oil displacing water, oil-injection alone, water-wet core)

Integrating term by term of Eq.(19) gives

$$\frac{L-x}{L} = \frac{k k_{ro}|_{S_{iw}} AP_d}{Lq_o \mu_o} \left\{ (S_w^*)^{-\frac{1}{\lambda}} - \right.$$

$$\frac{2\lambda^2(\lambda+2)(6\lambda^2+\lambda+1)}{(\lambda^2-1)(4\lambda^2-1)(3\lambda+1)} + \frac{2}{\lambda-1}(S_w^*)^{1-\frac{1}{\lambda}} - \frac{1}{2\lambda-1}(S_w^*)^{2-\frac{1}{\lambda}} + \frac{1}{\lambda+1}(S_w^*)^{1+\frac{1}{\lambda}} - \frac{2}{2\lambda+1}(S_w^*)^{2+\frac{1}{\lambda}} + \frac{1}{3\lambda+1}(S_w^*)^{3+\frac{1}{\lambda}} \} \quad (20)$$

(oil displacing water, oil-injection alone, water-wet core)

Using this equation, Fig.3 shows, as an example, the normalized water saturation profiles using  $\lambda = 2.1$  at different values of  $k k_{ro}|_{S_w} AP_d / Lq_o \mu_o$ .

In Fig.3, the inlet-end water-saturation is governed by Eq.(20) where  $x$  is set to zero:

$$1 = \frac{k k_{ro}|_{S_w} AP_d}{Lq_o \mu_o} \left\{ (S_{w,inlet}^*)^{-\frac{1}{\lambda}} - \frac{2\lambda^2(\lambda+2)(6\lambda^2+\lambda+1)}{(\lambda^2-1)(4\lambda^2-1)(3\lambda+1)} + \frac{2}{\lambda-1}(S_{w,inlet}^*)^{1-\frac{1}{\lambda}} - \frac{1}{2\lambda-1}(S_{w,inlet}^*)^{2-\frac{1}{\lambda}} + \frac{1}{\lambda+1}(S_{w,inlet}^*)^{1+\frac{1}{\lambda}} - \frac{2}{2\lambda+1}(S_{w,inlet}^*)^{2+\frac{1}{\lambda}} + \frac{1}{3\lambda+1}(S_{w,inlet}^*)^{3+\frac{1}{\lambda}} \right\} \quad (21)$$

This is a nonlinear equation which can be solved numerically. The solution is shown in Fig.4 where  $S_{w,inlet}^*$  is plotted as a function of  $k k_{ro}|_{S_w} AP_d / Lq_o \mu_o$  for  $\lambda = 1.5$  to 2.9.

**Average Water Saturation** - The average water saturation over the whole core (presumably close to interstitial level except in the vicinity of the outlet end) can be calculated as follows (note that the water saturations are all normalized):

$$\bar{S}_{iw}^* = \frac{1}{L} \int_0^L S_w^* dx = \frac{1}{L} \int_{S_{w,inlet}^*}^{S_w^*} S_w^* \left( \frac{dS_w^*}{dx} \right)^{-1} dS_w^* = \frac{k k_{ro}|_{S_w} AP_d}{Lq_o \mu_o} \times \int_{S_{w,inlet}^*}^1 \left\{ (1-S_w^*)^2 \left[ 1 - (S_w^*)^{\frac{2}{\lambda}+1} \right] / \lambda (S_w^*)^{\frac{1}{\lambda}} \right\} dS_w^* \quad (22)$$

This equation can be expanded and integrated term by term to give

$$\bar{S}_{iw}^* = \left[ \frac{2\lambda^2(\lambda+2)(18\lambda^2+\lambda+1)}{(\lambda-1)(4\lambda^2-1)(9\lambda^2-1)(4\lambda+1)} \right] X$$

$$\begin{aligned} & -XS_{w,inlet}^* \left( \frac{S_{w,inlet}^*}{\lambda-1} - \frac{2S_{w,inlet}^{*2}}{2\lambda-1} + \frac{S_{w,inlet}^{*3}}{3\lambda-1} \right) \\ & + XS_{w,inlet}^* \left( \frac{S_{w,inlet}^{*2}}{2\lambda+1} - \frac{2S_{w,inlet}^{*3}}{3\lambda+1} + \frac{S_{w,inlet}^{*4}}{4\lambda+1} \right) \end{aligned} \quad (23)$$

with  $X \equiv \frac{k k_{ro}|_{S_w} AP_d}{Lq_o \mu_o}$

With the solutions of Eq.(21) presented in Fig.4, Eq.(23) is used to compute the normalized interstitial water saturation for different values of  $\lambda$  and  $k k_{ro}|_{S_w} AP_d / Lq_o \mu_o$  as shown in Fig.5.

**Average Relative Permeability** - Now we continue to discuss the pressure drop in the core sample. Because of steady state and no water injection, the pressure drop in the core at an arbitrary distance  $x$  can be obtained by integrating the Darcy's equation for oil:

$$\begin{aligned} \Delta P|_x &= p|_x - p|_0 = -\frac{q_o \mu_o}{Ak} \int_0^x \frac{1}{k_{ro}} dx \\ &= -\frac{q_o \mu_o}{Ak} \int_0^x \frac{1}{k_{ro}} \frac{dx}{dS_w^*} dP_c \\ &= \frac{q_o \mu_o}{Ak} \int_{P_c(S_{w,inlet}^*)}^{P_c(S_w^*)} \frac{1}{k_{ro}} \left( \frac{Ak k_{ro}}{q_o \mu_o} \right) dP_c \\ &= \int_{P_c(S_{w,inlet}^*)}^{P_c(S_w^*)} dP_c = P_d \left[ (S_w^*)^{-\frac{1}{\lambda}} - (S_{w,inlet}^*)^{-\frac{1}{\lambda}} \right] \quad (24) \end{aligned}$$

At given  $k k_{ro}|_{S_w} AP_d / Lq_o \mu_o$  and  $\lambda$  values, Fig.5 shows  $S_w^*$  being a function of  $x$ , and the value of  $S_{w,inlet}^*$  can be determined from Fig.4. Thus, using Eq.(24), the pressure gradient curve (in dimensionless form) can be plotted as shown in Fig.6. Fig.6 shows that a significant pressure drop exists across the last 20% of the core length for all situation considered. The right-hand side end point of each curves (i.e., the outlet end) in Fig.6 is related to the ratio of the actual terminal relative permeability to that of the averaged, as now discussed.

Steady-state terminal oil relative permeability, in the laboratory, is calculated based on the pressure drop over the entire core. This calculation requires correction because of the capillary end effect. Denote the average relative perme-

ability (based on the entire core pressure drop  $(\Delta P|_{x=L} = \Delta P_L)$ ,  $\bar{k}_{ro}$ , from Darcy's law and using Eq.(24),

$$\bar{k}_{ro}|_{\bar{S}_{iw}} = \frac{Lq_o\mu_o}{k(-\Delta P_L)A} = \frac{Lq_o\mu_o}{kP_dA} \left[ (S_{w,inlet}^*)^{-\frac{1}{\lambda}} - 1 \right]^{-1} \quad (25)$$

or,

$$\frac{k_{ro}|_{S_{iw}}}{\bar{k}_{ro}|_{\bar{S}_{iw}}} = X \left[ (S_{w,inlet}^*)^{-\frac{1}{\lambda}} - 1 \right]; X \equiv \frac{kk_{ro}|_{S_{iw}} AP_d}{Lq_o\mu_o} \quad (26)$$

Eq.(26) represents the ratio of the *actual* terminal oil relative permeability to that of the averaged  $\bar{k}_{ro}$ . This ratio is graphically shown in Fig.7. Fig.7 shows that the *actual* oil relative permeability ( $k_{ro}$  @  $S_{iw}$ ) at terminal condition is greater than the averaged  $\bar{k}_{ro}$  @  $\bar{S}_{iw}$ . Physically, this means that the higher pressure gradient near the outlet end caused by the capillary end effect results in a lower averaged relative permeability.

**Corrections of Terminal Oil Relative Permeability Computation** - Based on the previous calculations, the terminal oil relative permeability ratio,  $k_{ro}/\bar{k}_{ro}$ , can be expressed in terms of measurable quantities.

The ratio of the two quantities shown as the x-coordinate in Fig.8 and Fig.9, is  $P_d/|\Delta P_L|$ , the ratio of the displacement pressure to the viscous pressure drop over the entire core:

$$\left( \frac{kk_{ro}|_{S_{iw}} AP_d}{Lq_o\mu_o} \right) \div \left( \frac{k\bar{k}_{ro}|_{\bar{S}_{iw}} AP_d}{Lq_o\mu_o} \right) = \frac{k\bar{k}_{ro}|_{\bar{S}_{iw}} AP_d}{Lq_o\mu_o} = \frac{P_d}{|\Delta P_L|} \quad (27)$$

Fig.8 shows  $k_{ro}|_{S_{iw}}/\bar{k}_{ro}|_{\bar{S}_{iw}}$  as a function of  $P_d/|\Delta P_L|$  for various  $\lambda$ . Based on measured  $k\bar{k}_{ro}|_{\bar{S}_{iw}} AP_d / Lq_o\mu_o$  (i.e.,  $P_d/|\Delta P_L|$ ) and  $\lambda$ , we can find the value of  $k_{ro}|_{S_{iw}}/\bar{k}_{ro}|_{\bar{S}_{iw}}$  from Fig.8. This value and the averaged  $\bar{k}_{ro}|_{\bar{S}_{iw}}$  can be used to compute the actual terminal oil relative permeability  $k_{ro}|_{S_{iw}}$ .

**Corrections of Interstitial Water Saturation Computation** - Fig.9 shows the normalized average interstitial water saturation,  $\bar{S}_{iw}^*$ , as a function of the measurable  $k\bar{k}_{ro}|_{\bar{S}_{iw}} AP_d / Lq_o\mu_o$

(i.e.,  $P_d/|\Delta P_L|$ ) and  $\lambda$ . Based on measured  $k\bar{k}_{ro}|_{\bar{S}_{iw}} AP_d / Lq_o\mu_o$  and  $\lambda$ , we find the value of  $\bar{S}_{iw}^*$  using Fig.9. From Eq.(12), we have

$$\bar{S}_{iw}^* = \frac{\bar{S}_{iw} - S_{iw}}{1 - S_{iw} - S_{or}} \quad (28)$$

Solving for  $S_{iw}$ ,

$$S_{iw} = \frac{\bar{S}_{iw} - \bar{S}_{iw}^*(1 - S_{or})}{1 - \bar{S}_{iw}^*} \quad (29)$$

For known values of  $\bar{S}_{iw}^*$  (from Fig.9),  $\bar{S}_{iw}$  (measured) and  $S_{or}$  (measured), the actual interstitial water saturation at the terminal condition,  $S_{iw}$  (free of end effect) can be calculated using Eq.(29).

**Examples of Relative Permeability and Saturation Corrections** - The computations of corrected terminal oil relative permeability and interstitial water saturation are demonstrated in this section. Values obtained from Figs. 8 and 9 using  $\lambda = 2.1$ , a typical value for consolidated sandstone, are tabulated in Table 1. Using Fig.4, the inlet water saturation values are also tabulated.

Table 1 shows that the higher the capillary-to-viscous pressure ratio ( $P_d/|\Delta P_L|$ ), the more significant are corrections in  $S_{iw}$  and  $k_{ro}$ . In an example shown in the table ( $P_d/|\Delta P_L| = 0.4$ , the capillary pressure being quite significant), the averaged relative permeability is 81% lower than the actual value, and the averaged interstitial water saturation is 0.164PV higher than the actual value (i.e.,  $\bar{S}_{iw} - S_{iw} = 0.164$ ).

### SIMULTANEOUS ESTIMATION OF REL. PERM. AND CAP. PRESSURE

In this section, we will show how to simultaneously estimate the relative permeabilities and capillary pressure of a core sample, if the averaged and actual values of interstitial water saturation and terminal oil relative permeability are given. To obtain the latter information, we conducted a coreflood experiment using a carbonate core sample, which possesses water-wet characteristics at reservoir temperature.

The core dimensions and the experimental conditions are:

$$\begin{aligned} L &= 10 \text{ cm}, D = 1.83 \text{ cm}, k = 5 \text{ md}, \\ \phi &= 22.5\%, T = 150 \text{ }^\circ\text{F}, \mu_o = 6 \text{ cp}, \\ q_o &= 1.389\text{E-}4 \text{ cm}^3/\text{sec} \end{aligned}$$

The experiment was monitored by microwave attenuation techniques along every centimeter of the core for *in-situ* saturation profile information (see Fig.10). The experiment protocol and the results are the following:

**Step 1.** Oilflood ( $q_o = 0.5$  cc/hr) a core that initially has a mean residual oil saturation,  $S_{or} = 0.251$ . At the end of oilflood, in the presence of capillary end effect, the averaged interstitial water saturation ( $\bar{S}_{iw}$ ) is 0.324, and the averaged terminal oil relative permeability,  $\bar{k}_{ro}|_{\bar{S}_{iw}} = 0.51$ .

**Step 2.** Use a water-wet porous plate at the core outlet end. Transform the constant-rate injection mode into the constant-pressure mode of oil injection. In this way, the nonuniform water saturation profile becomes uniform (see Fig.10). At this point, we found the *true* interstitial water saturation,  $S_{iw} = 0.292$ .

**Step 3.** Remove the porous plate, and again conduct a constant rate oil injection ( $q_o = 0.5$  cc/hr) to determine the *true* terminal oil relative permeability (i.e., without the capillary end effect). We found  $k_{ro}|_{S_w} = 0.65$ .

The experimental results give us

$$\frac{k_{ro}|_{S_{iw}}}{\bar{k}_{ro}|_{\bar{S}_{iw}}} = \frac{0.65}{0.51} = 1.275 \quad (30)$$

$$\bar{S}_{iw}^* = \frac{\bar{S}_{iw} - S_{iw}}{1 - S_{iw} - S_{or}} = \frac{0.324 - 0.292}{1 - 0.292 - 0.251} = 0.07 \quad (31)$$

Interpolating the value of  $\lambda$  from Figs. 8 and 9 simultaneously using Eqs.(30) and (31), we found

$$\lambda = 2.3, \text{ and } \frac{k \bar{k}_{ro}|_{\bar{S}_{iw}} A P_d}{L q_o \mu_o} = 0.18 \quad (32)$$

which further gives the value of the threshold pressure,  $P_d$ :

$$\begin{aligned} P_d &= \frac{0.18 L q_o \mu_o}{k \bar{k}_{ro}|_{\bar{S}_{iw}} A} = \frac{(0.18)(10)(0.5/3600)(6 \times 0.01)}{(5 \times 9.87 \times 10^{-12})(0.51)(2.63)} \times \\ &\frac{\text{psi}}{68947.57 \text{ dyne/cm}^2} = 3.28 \text{ psi} \quad (33) \end{aligned}$$

Eqs.(11), (16), and (17), that predict relative permeabilities and capillary pressure, become

$$P_c \text{ (psi)} = 3.28 \times \left( \frac{S_w - 0.292}{0.457} \right)^{-1/2.3} \quad (34)$$

$$\begin{aligned} k_{ro} &= 0.65 \times \left[ 1 - \left( \frac{S_w - 0.292}{0.457} \right) \right]^2 \\ &\times \left[ 1 - \left( \frac{S_w - 0.292}{0.457} \right)^{1.87} \right] \quad (35) \end{aligned}$$

$$k_{rw} = (k_{rw}|_{S_{or}} = 0.06) \times \left( \frac{S_w - 0.292}{0.457} \right)^{3.87} \quad (36)$$

In order to check the validity of these equations, we conducted separate measurements for capillary pressure and steady-state water/oil relative permeabilities. The comparison between values from predictions and measurements are shown in Figs. 11 and 12.

Fig.11 shows the comparison of capillary pressure prediction (Eq.(34)) with data from three different measurements: (a) reservoir-condition centrifuge experiment, (b) reservoir-condition porous-plate experiment through the use of microwave attenuation for water saturation determination, and (c) ambient-condition mercury-injection experiments rescaled to the reservoir condition. Our prediction using Eq.(34) provides an overall agreement with the three different sets of data.

Fig.12 shows the comparison between the predicted relative permeabilities (Eqs.(35) and (36)) with that measured in a reservoir-condition steady-state experiment using microwave attenuation for *in-situ* water saturation determination. Again, the predicted curves agree well with the measurement.

To double check the calculations, we substitute the values of  $P_d$  and  $\lambda$  from Eqs.(32) and (33) for Eq.(19), the profile equation, to determine the saturation profile. The predicted profile can be compared with the measured saturation profile (shown earlier in Fig.10) as a final check. Fig.13 shows this comparison. Again, the theory agrees well with the experiment.

## SUMMARY AND CONCLUSIONS

In this work, we have addressed how capillary end effects can influence the computation of relative permeability and saturation in coreflood experiments. To illustrate, we studied the situations of oil displacing water in a water-wet core at the terminal condition as an example.

- We showed how to convert the averaged terminal oil relative permeability to the actual oil relative permeability. This correction, in some cases we studied, can be very significant (in the order of 100%) when the capillary force is of the same order of magnitude as the viscous force.
- We showed how to compute the actual interstitial water saturation from an averaged value. The correction to the computation of  $S_{iw}$  is found even more significant than that needed for the terminal relative permeability.

- We also demonstrated how to simultaneously estimate relative permeabilities and capillary pressure in a drainage process, based on terminal-condition measurements with and without the capillary end effect. The estimated relative permeabilities and capillary pressure were in good agreement with experimental data from different sources. When applying this simultaneous estimation technique, the capillary-induced nonuniform saturation profile information should be obtained from *in-situ* scanning methods.

## ACKNOWLEDGMENT

We thank Mobil management for permission to publish this paper. We thank the technical discussions with Rafi Al-Hussainy and George Hirasaki.

**TABLE 1. CAPILLARY END EFFECTS CALCULATION FOR OIL DISPLACEMENT OF WATER IN A WATER-WET CORE USING  $\lambda = 2.1$**

$P_d/ \Delta P_L $	Ratio of Dynamic Press. Drop (viscous) and Displ. Press., $ \Delta P_L /P_d$	Normalized Inlet Water Saturation, $S_{w,inlet}^*$	Normalized Avg. Water Saturation $\bar{S}_{iw}^*$	For $\bar{S}_{iw} = 20\%$ , $S_{or} = 0$ (primary drainage) Value of $S_{iw}$	Rel. Perm. Correction: $\frac{k_{ro} _{S_{iw}}}{\bar{k}_{ro} \bar{S}_{iw}}$
0.01	100	4.2E-5	4.5E-3	19.64%	1.02
0.02	50.0	2.5E-4	8.8E-3	19.29%	1.03
0.04	25.0	1.1E-3	1.8E-2	18.53%	1.07
0.08	12.5	4.2E-3	3.6E-2	17.01%	1.13
0.10	10.0	6.7E-3	4.5E-2	16.23%	1.17
0.20	5.00	2.3E-2	8.8E-2	12.28%	1.36
0.30	3.33	4.6E-2	1.3E-1	8.05%	1.58
0.40	2.50	7.2E-2	1.7E-1	3.61%	1.81

## REFERENCES

- <sup>1</sup> Richardson, J. G., Kerver, J. K., Hafford, J. A., and Osoba, J. S., "Laboratory Determination of Relative Permeability," *Petroleum Transactions, AIME*, **195**, 187-196 (1952).
- <sup>2</sup> Brooks, R. H., and Corey, A. T., "Hydraulic Properties of Porous Media," *Hydrology Papers of Colorado State University*, No. 3. (1964).
- <sup>3</sup> Purcell, W. R., "Capillary Pressures - Their Measurement Using Mercury and the Calculation of Permeability Therefrom," *Petroleum Transactions, AIME*, February, 39-48 (1949).
- <sup>4</sup> Burdine, N. T., "Relative Permeability Calculations from Pore Size Distribution Data," *Petroleum Transactions, AIME*, Vol. 198 71-78 (1953).
- <sup>5</sup> Corey, A. T., "The Interrelation Between Gas and Oil Permeabilities," *Producers Monthly*, November, 38-41 (1954).
- <sup>6</sup> Honarpour, M. M., Koederitz, L., and Harvey, A. H., *Relative Permeability of Petroleum Reservoirs*, 1986, CRC Press.

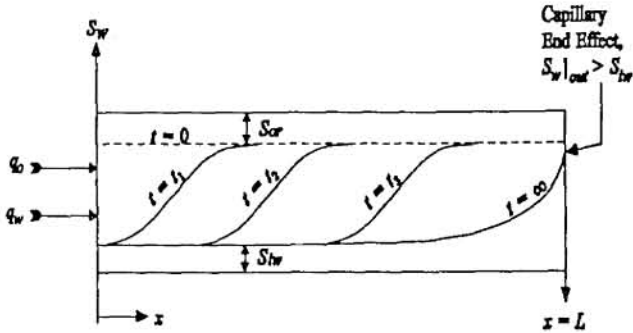


Figure 1. The capillary end effect in an oil-water co-injection experiment. The core, assuming water-wet, was initially saturated with water, with or without  $S_{or}$ .

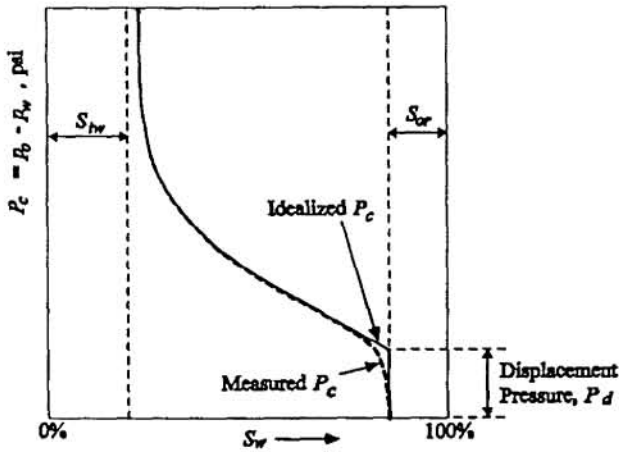


Figure 2. In oil-displacing-water case, the measured capillary curve (dashed) can be represented by an idealized curve (solid). The intercept of the idealized curve at residual oil saturation is the displacement pressure,  $P_d$ .

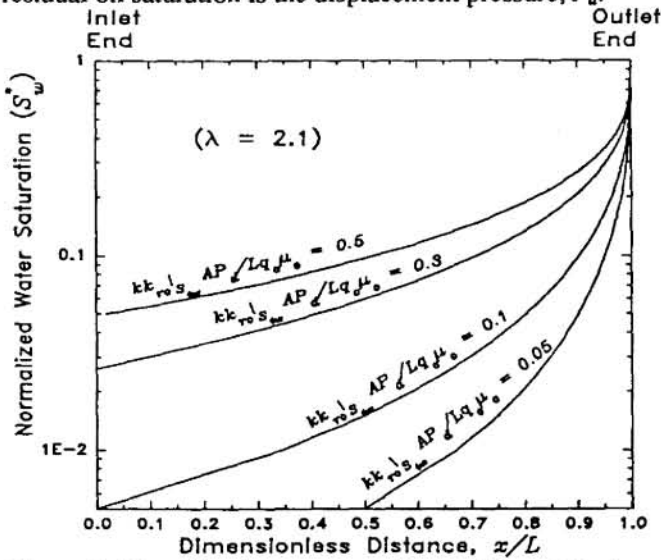


Figure 3. Normalized water saturation profiles of single-phase oil injection displacing water in a water-wet core for  $\lambda = 2.1$  and different values of  $k k_{ro}|_{S_w} AP_d / L q_o \mu_o$ .

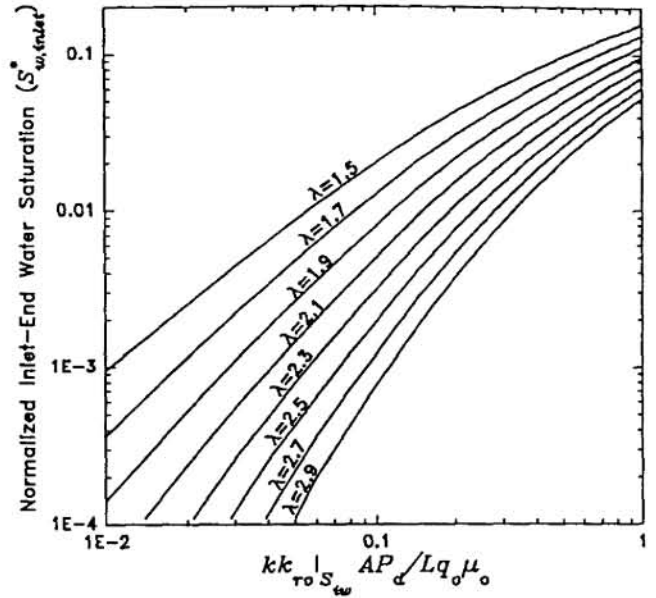


Figure 4. Normalized inlet-end water saturation as a function of  $k k_{ro}|_{S_w} AP_d / L q_o \mu_o$  for single-phase oil displacing water (water-wet core;  $1.5 \leq \lambda \leq 2.9$ ).

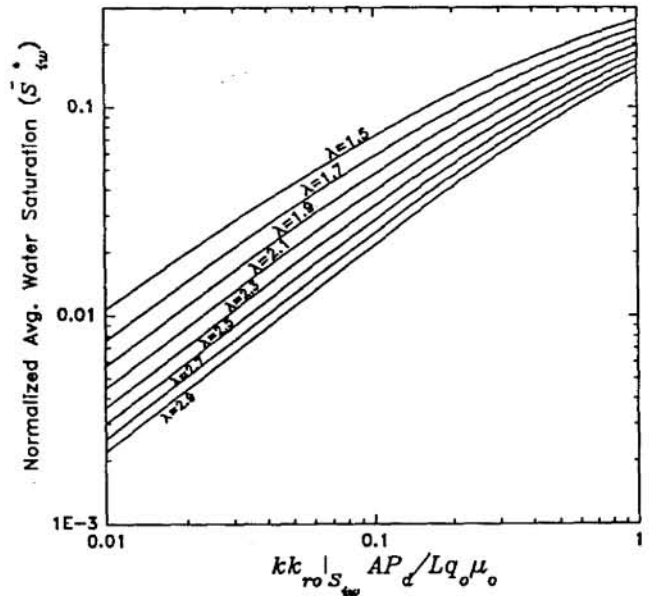


Figure 5. Normalized average water saturation as a function of  $k k_{ro}|_{S_w} AP_d / L q_o \mu_o$  for single-phase oil displacing water (water-wet core;  $1.5 \leq \lambda \leq 2.9$ ).

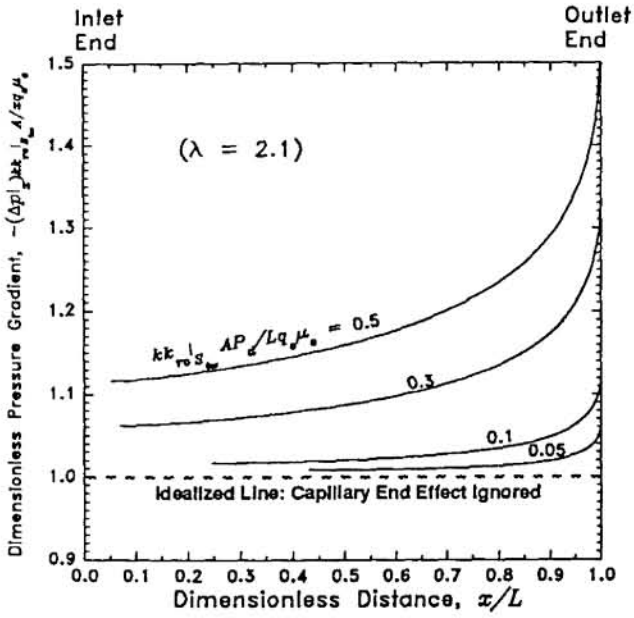


Figure 6. Pressure gradient,  $(-\Delta p|_x) k k_{ro}|_{S_{tw}} A / x q_o \mu_o$ , as a function of distance from the injection end,  $x/L$ . Condition considered: single-phase oil displacing water (water-wet core;  $\lambda = 2.1$ ).

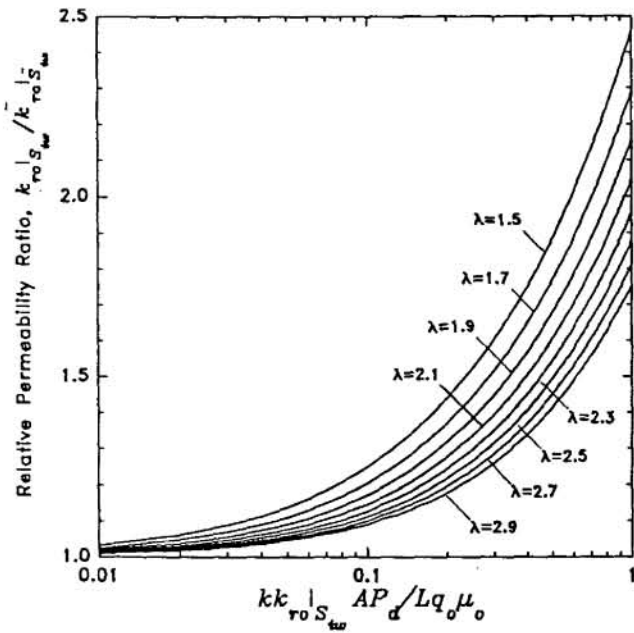


Figure 7. Ratio of actual terminal oil relative permeability to the averaged value as a function of  $k k_{ro}|_{S_{tw}} AP_d / L q_o \mu_o$  for  $1.5 \leq \lambda \leq 2.9$ . The averaged terminal oil relative permeability is calculated based on the total pressure drop across a core sample.

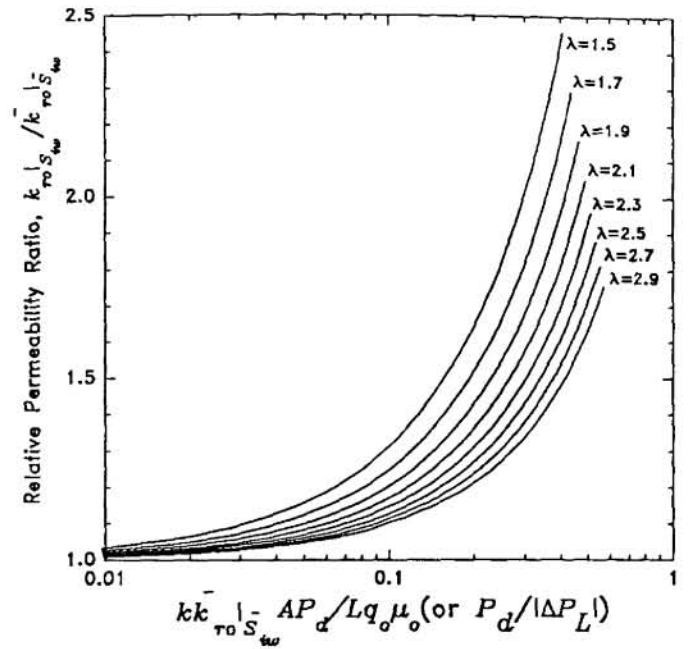


Figure 8. Ratio of the actual terminal oil relative permeability to the averaged terminal oil relative permeability as a function of  $P_d / |\Delta P_L|$  for  $1.5 \leq \lambda \leq 2.9$ .

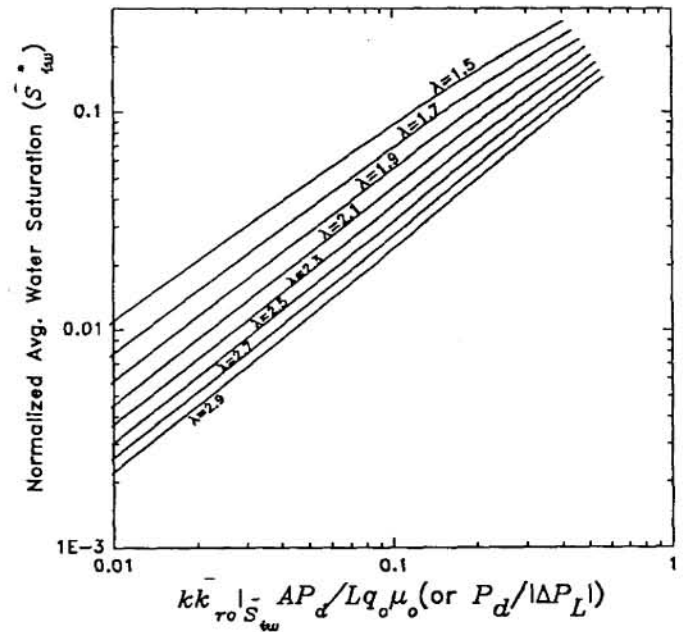


Figure 9. Normalized average water saturation as a function of  $P_d / |\Delta P_L|$  for  $1.5 \leq \lambda \leq 2.9$ .

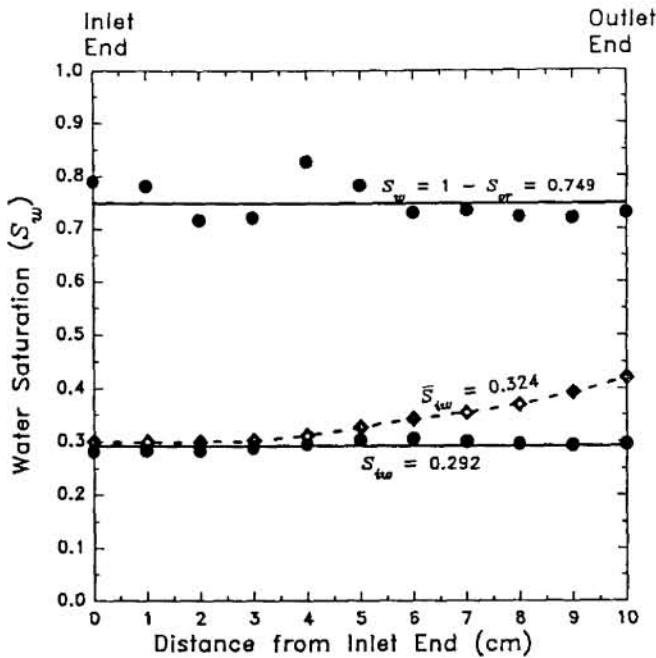


Figure 10. Water saturation profiles before and after the coreflood experiments. Initial condition: top bullets with a mean  $S_w = 0.749$ ; final condition with the capillary end effect: open diamonds with an average  $\bar{S}_{iw} = 0.324$ ; final condition without the capillary end effect: bottom bullets with a mean  $S_{iw} = 0.292$ . Saturation profiles are obtained by microwave attenuation techniques.

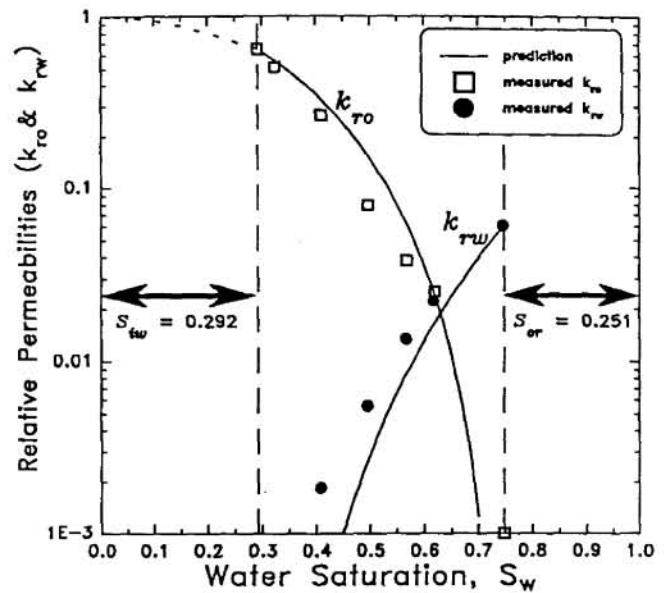


Figure 12. Comparison between the theoretically predicted relative permeabilities with the experimental data. The experiment was conducted at reservoir condition in steady-state mode.

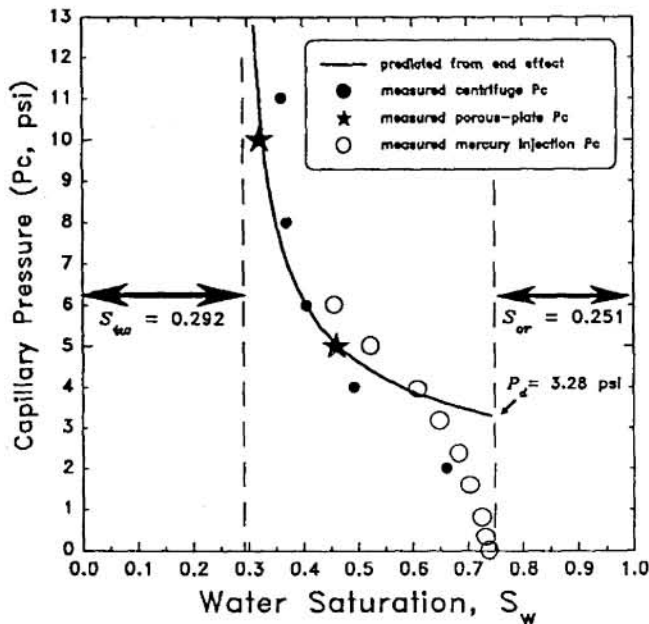


Figure 11. Comparison between the theoretically predicted capillary pressure with the measured ones from centrifuge, porous-plate, and mercury-injection experiments.

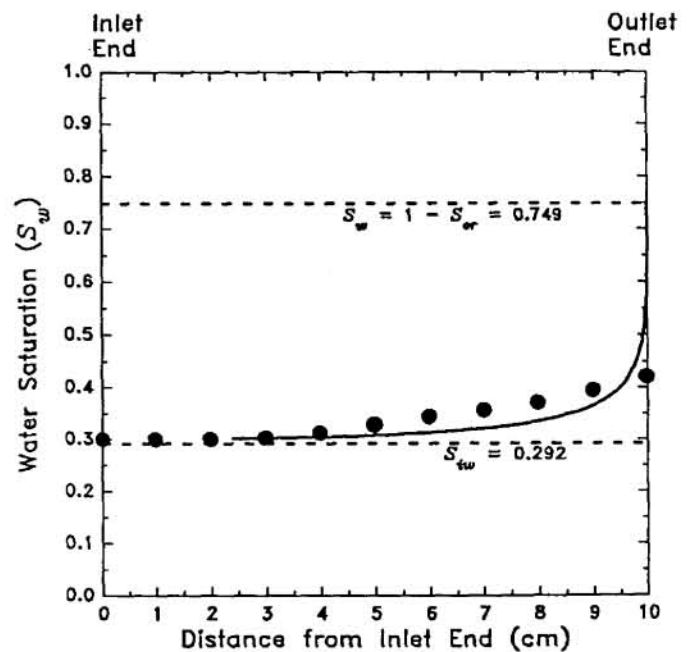


Figure 13. Comparison between the predicted capillary-end-effect saturation profile with that measured using microwave attenuation techniques. Solid Curve: predicted, bullets: measured values.